ELSEVIER

Physica A 213 (1995) 451–464

PHYSICA A

Coexistence of symmetric and parity-broken dendrites in a channel

Raz Kupferman[a], David A. Kessler[b], Eshel Ben-Jacob[a]

[a] *School of Physics and Astronomy, Raymond and Beverly Sackler Faculty of Exact Sciences, Tel Aviv University, Tel Aviv 69978, Israel*

[b] *Department of Physics, Bar-Ilan University, Ramat Gan 52900, Israel*

Received 5 July 1995

Abstract

We numerically solve the steady-state equation and the stability spectrum for solidification in a channel. For a large range of parameters stable symmetric and stable parity-broken solutions coexist. The branches of parity-broken solutions are found to originate from the symmetric solutions through standard bifurcations.

1. Introduction

The problem of dendritic growth in a channel [1,2] is one of the classical problems of pattern formation [3–6]. It incorporates in various limits the cases of a free dendrite, and of the Saffman-Taylor finger. Both of these limiting cases have been understood in the context of the paradigm of microscopic solvability [7,8]. Much progress has also been made working out the interpolating case, using both numerical [1] and approximate analytical [2] methods. However, it has recently been discovered that the spectrum of solutions is much richer than had previously been supposed. Brener *et al.* [9] and Ihle and Müller-Krumbhaar [10] found asymmetric (parity-broken) dendrites. Such patterns were observed also in numerical simulations of the phase-field model (Fig. 1) [11]. In this paper we use numerical boundary-integral techniques to extract additional information about this new class of solutions and determine their stability.

Parity-broken dendrites are important not only in their own right, but also for the role they may play in organizing more complex morphologies. The search for parity-broken solutions was motivated by an attempt to understand the dense-branching morphology [12] seen at large undercooling and small anisotropy [13,11]. The existence of such

0378-4371/95/$09.50
SSDI 0378-4371(94)00210-X

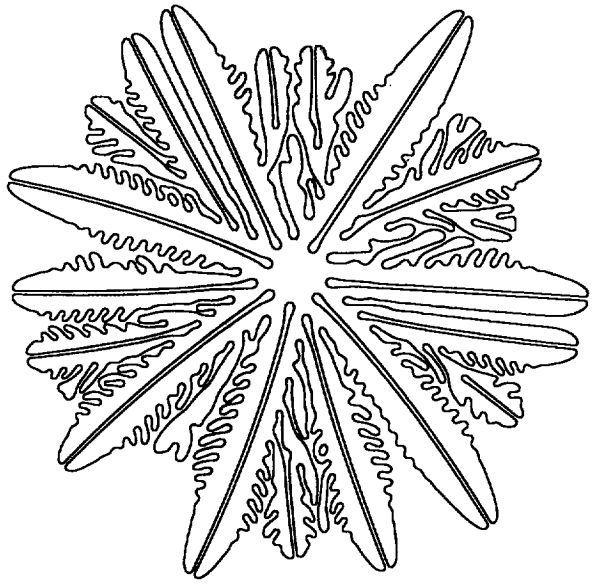

Fig. 1. The solid-liquid interface for a numerical simulation of the phase-field model under isotropic conditions. Couples of mirror-image parity-broken dendrites grow at constant velocity. The direction of propagation was shown to be independent of any source of anisotropy. It seems as if a mechanism of mutual stabilization acts by the creation of an effective half-space for each asymmetric dendrite.

solutions allows for the existence of a front propagating at constant velocity. The velocity of propagation of these fingers may provide a natural scale for the velocity of the propagating front [13].

One of the critical issues in unraveling the puzzle of morphological selection is the coexistence of two different linearly stable patterns for the same parameters. Such coexistence has been hypothesized on general grounds by Ben-Jacob *et al.* [14], and has been observed by Shochet and Ben-Jacob [15] in numerical simulations of the diffusion-transition algorithmic model [16]. However, the origins of such coexistence from a bifurcation viewpoint has not been clear. Typically, we should expect new solutions to arise from bifurcations, which result in the instability of one of the branches. In the problem at hand, Ihle and Müller-Krumbhaar reported coexistence of both stable symmetric and parity-broken fingers for a finite range of their parameters. It is important to investigate further the range of such coexistence, and also to understand its origins.

The existence of parity-broken solutions at all in this system is surprising given their non-existence in the two limiting cases of the free dendrite and the Saffman-Taylor finger [17]. On the other hand, parity-broken solutions have been found in eutectic systems [18], and in directional solidification [19]. It is important to distinguish between these parity-broken states, and the parity-broken states associated with transverse drift [20]. Considering an infinite array of symmetric fingers, the present parity-broken states arise from an instability of Bloch wave number $k = \pi$, whereas the drift states are associated with a $k = 0$ instability. The present case is qualitatively different from eutectics and

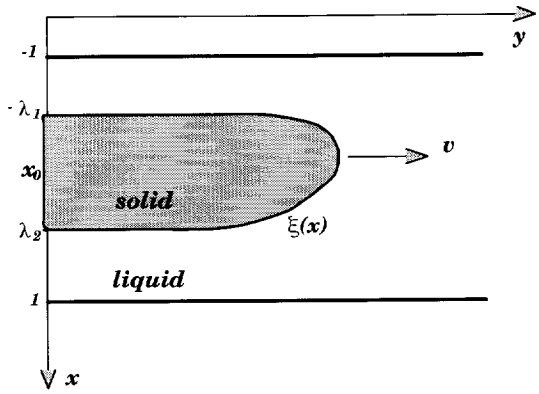

Fig. 2. A finger growing in a two-dimensional channel.

directional solidification in that the cells here are of infinite depth.

Some of the questions we plan to address in this paper are: (i) the origins of the parity-broken solutions in terms of bifurcations from known solutions, (ii) the existence of additional branches of parity-broken solutions, and (iii) the stability of the various branches, and its relation to the bifurcations. In particular, the mapping of the full structure of solutions resolves some of the open questions raised by Ihle and Müller-Krumbhaar that could not be settled in the framework of the dynamical approach.

2. The free-boundary model

In this section, we review the well-known evolution equations for two-dimensional fingers in a channel, growing under chemical diffusion-limited conditions. We consider a crystal growing from a supersaturated solution in a two-dimensional channel of width $2a$ (Fig. 2). The channel is directed along the y-axis. The dimensionless solute concentration field is defined as

$$u(x,y,t) = \frac{c_\infty - c(x,y,t)}{1 - c_{eq}}, \tag{1}$$

where c_{eq} is the equilibrium concentration at phase coexistence, and c_∞ is the solute concentration far from the growing solid. In the solid then, u is equal to $\Delta \equiv (c_\infty - c_{eq})/(1-c_{eq})$, the dimensionless supersaturation. The location of the interface is denoted by $\zeta(x,t)$. We adopt dimensionless units with length measured in units of the channel half-width, a, and time measured in units of a^2/D, where D is the diffusion constant of solute in the solution. The growth dynamics is assumed to be described by the one-sided free boundary model (for a conserved order-parameter). In the solution, u satisfies the diffusion equation,

$$\frac{\partial u}{\partial t} = \nabla^2 u. \tag{2}$$

The interfacial boundary conditions are mass conservation

$$\hat{n} \cdot \nabla u(x, \zeta(x,t), t) = -(1 - d_0 \kappa(x,t))\, v_n(x,t), \tag{3}$$

where $\hat{n}$ is the interfacial normal unit vector, κ is the curvature, and d_0 is the capillary length, and the Gibbs-Thompson local equilibrium relation,

$$u(x, \zeta(x,t), t) = \Delta - d_0 \kappa, \tag{4}$$

(we neglect the kinetic effects). Four-fold surface tension anisotropy is included by setting $d_0(\theta) = d_0(1 - \epsilon \cos 4\theta)$, where ϵ controls the level of anisotropy, and θ is the angle between the interface normal and the channel orientation. Finally, impermeable walls are assumed, implying $\partial u/\partial x = 0$ for $x = \pm 1$.

As is standard, we transform Eqs. (2)-(4) into an integro-differential equation for $\zeta(x,t)$, in a frame of reference moving at velocity v along the channel axis,

$$\Delta = \int_{-\infty}^{t} dt' \int dx' \left[2p + \dot{\zeta}(x',t')\right] \mathcal{G}\Big(x, \zeta(x,t), t; x', \zeta(x',t'), t'\Big)$$
$$- \int_{-\infty}^{t} dt' \int ds(t')\, d_0(s,t') \kappa(s,t') \frac{\partial \mathcal{G}}{\partial n'}\Big(x, \zeta(x,t), t; x(s), \zeta(s,t'), t'\Big). \tag{5}$$

The integration ds is along the solid-liquid interface, the Péclet number, $p = av/2D$, is the dimensionless velocity, and $\mathcal{G}(\mathbf{r}, t; \mathbf{r}', t')$ is the Green's function given by

$$\mathcal{G}(\mathbf{r}, t; \mathbf{r}', t') = \sum_{n=-\infty}^{\infty} \frac{\Theta(t-t')}{4\pi(t-t')} \exp\left\{-\frac{\left[(y-y') + 2p(t-t')\right]^2}{4(t-t')}\right\}$$
$$\times \left\{\exp\left[-\frac{(x+4n-x')^2}{4(t-t')}\right] + \exp\left[-\frac{(2+4n-x-x')^2}{4(t-t')}\right]\right\}, \tag{6}$$

($\Theta(t)$ is the Heaviside step function). In fact, the integral over $\partial \mathcal{G}/\partial n$ gives rise to a discontinuity in u analogous to that of a dipole layer, hence $\zeta(x,t)$ has to be taken slightly inside the solid.

3. Numerical method

3.1. Steady-state solutions

If a steady-state solution is assumed the integration over t' in Eq. (5) can be carried out explicitly. The stationary interfacial shape, $\zeta(x)$, then satisfies the following equation,

$$\Delta = -\int ds\, d_0(s) \kappa(s) \frac{\partial G}{\partial n}(x, \zeta(x); x(s), \zeta(s))$$

$$+2p\int dx' G\left(x,\zeta(x);x,\zeta(x')\right), \tag{7}$$

with

$$G(\mathbf{r};\mathbf{r'}) = \frac{1}{2\pi}e^{-p(y-y')}\sum_{n=-\infty}^{\infty}\left\{K_0\left(p\sqrt{(x+4n-x')^2+(y-y')^2}\right)\right.$$
$$\left.+K_0\left(p\sqrt{(2+4n-x-x')^2+(y-y')^2}\right)\right\}. \tag{8}$$

To solve Eq. (7) numerically for asymmetric solutions, we generalize the boundary integral method developed by Kessler et al. for symmetric solutions [1]. Parity-broken dendrites are fingers approaching negative infinity at $x = -\lambda_1, \lambda_2$. As the asymptotic crystal width is constrained by global solute conservation, $\lambda_1 + \lambda_2 = 2\Delta$, this introduces one additional degree of freedom in the solution. Similar to the symmetric case, the asymptotic behavior of $\zeta(x)$ at $\zeta \to -\infty$. is given by

$$x(\zeta) \sim \lambda_2 - C_2 e^{\alpha_2\zeta} - D_2 e^{2\alpha_2\zeta}, \tag{9}$$

with $\beta_2 = \sqrt{\alpha_2^2 + 2p\alpha_2}$ and $\gamma_2 = \sqrt{4\alpha_2^2 + 4p\alpha_2}$, with parallel expressions obtaining at $x \to -\lambda_1$. The exponential approach rate, α_2, is the smallest root of

$$2p\cos\left[\beta_2(1-\lambda_2)\right] = d_0(1-\epsilon)\alpha_2\beta_2\sin\left[\beta_2(1-\lambda_2)\right]. \tag{10}$$

In order to operate on a bounded computational field, the interface is parameterized as $\zeta(x) = \zeta_0(x) + z(x)$, where the base curve, $\zeta_0(x)$, has the asymptotic behavior of the solution. Specifically, we take

$$\zeta_0(x) = \begin{cases} \dfrac{1}{\alpha_1}\log\sin\left[\dfrac{\pi}{2}\left(\dfrac{\lambda_1+x}{\lambda_1+x_0}\right)\right] - \dfrac{\pi^2(x-x_0)^2}{8\alpha_2(\lambda_2-x_0)}, & -\lambda_1 < x < x_0 \\ \dfrac{1}{\alpha_2}\log\sin\left[\dfrac{\pi}{2}\left(\dfrac{\lambda_2-x}{\lambda_2-x_0}\right)\right] - \dfrac{\pi^2(x-x_0)^2}{8\alpha_1(\lambda_1+x_0)}, & x_0 < x < \lambda_2 \end{cases}, \tag{11}$$

where $x_0 = (\lambda_2 - \lambda_1)/2$. The derivative of the computational field, $z(x)$, at the end point is then finite, and given by

$$z'(\lambda_2) = \frac{D_2}{\alpha_2 C_2^2} = \frac{\alpha_2\beta_2^2 d_0(1-\epsilon) + \gamma_2 p\tan\left[\gamma_2(1-\lambda_2)\right]}{2p\alpha_2 - 2\alpha_2^2\gamma_2 d_0(1-\epsilon)\tan\left[\gamma_2(1-\lambda_2)\right]}, \tag{12}$$

with a similar expression obtained for $z'(-\lambda_1)$.

The numerical procedure consists basically of discretizing $z(x)$ into N points, which together with p and λ_2, form a total of $N+2$ unknowns. For a correct implementation of the boundary integral technique, it is necessary for z and z' to be fixed at both end points, $-\lambda_1$ and λ_2. Whereas in the symmetric case, translational invariance could be used to fix $z(\lambda_1)$, with $z(\lambda_2)$ immediately determined by symmetry, here the boundary condition remains undetermined on one end. It turns out that the results of the numerical

procedure are practically insensitive to the value substituted for this missing boundary condition as long as it is kept fixed. The reason is that the procedure is equivalent to solving a second order ordinary differential equation with initial conditions given at $z = -\infty$. Local analysis near these points shows that any finite error will decay exponentially when shooting back toward the tip. The set of equations is completed by the $N - 2$ equations, obtained by evaluating Eq. (7) at the interior points. This non-linear algebraic set is then solved by Newton's method. The integrals entering into Eq. (7) are evaluated using a simple trapezoidal rule, which after accounting for the Green's function singularities, is accurate to $O(1/N^2)$. The quadratic convergence was used as a basic test for the entire procedure.

In many cases, it proved necessary to use mismatch functions in order to facilitate the numerical procedure. The method is to fix p and λ_2, relaxing one equation (for $x = x_0$), and allowing a discontinuity in $z(x)$ at this point. Thus, for each set of values (p, λ_2), there are two mismatch functions, $(\Delta z_0, \Delta z_0')$, and the remaining procedure is an ordinary root finding in this two-dimensional space.

3.2. *Linear stability operator*

In this section we describe the numerical procedure for calculating the stability spectrum of steady-state solutions. It is based on the method developed by Kessler and Levine which was already applied for free dendrites [21], and for Saffman-Taylor fingers [22]. Here, the perturbation equation is written in terms of longitudinal shifts, rather than normal shifts.

Once a steady-state solution, $\zeta(x)$ has been found, we set

$$\zeta(x,t) = \zeta(x) + \delta(x)e^{\omega t}, \tag{13}$$

and linearize the equation of motion, (5), about the small perturbation, $\delta(x)$. Integration over t' can again be carried out explicitly, yielding a non-linear eigenvalue equation for the amplification rate, ω,

$$\begin{aligned}
\omega \int dx'\, G_\omega \delta(x') = 2p &\int dx' \frac{\partial G_\omega}{\partial y'} \left[\delta(x) - \delta(x')\right] \\
&+ \int dx' \left[3d_0(x') \sin\theta - 4\epsilon d_0 \sin 4\theta \cos\theta\right] \kappa(x') \\
&\times \left(\sin\theta \frac{\partial G_\omega}{\partial x'} - \cos\theta \frac{\partial G_\omega}{\partial y'}\right) \delta'(x') \\
&+ \int dx'\, d_0(x') \cos^2\theta \left(\sin\theta \frac{\partial G_\omega}{\partial x'} - \cos\theta \frac{\partial G_\omega}{\partial y'}\right) \delta''(x') \\
&+ \int dx'\, d_0(x') \kappa(x') \\
&\times \left\{ \left(\tan\theta \frac{\partial^2 G_\omega}{\partial x' \partial y'} - \frac{\partial^2 G_\omega}{\partial y'^2}\right) \left[\delta(x) - \delta(x')\right] - \frac{\partial G_\omega}{\partial x'} \delta'(x') \right\},
\end{aligned} \tag{14}$$

where the ω-dependent Green's function, G_ω, is obtained by substituting $p \to \sqrt{p^2 + \omega}$ for the arguments of the Bessel functions in Eq. (8). We will use the standard *quasi-static approximation* neglecting the time dependence of the perturbation in all terms other than the velocity. Under this approximation the Green's functions are no longer ω-dependent, and the eigenvalue problem reduces to a standard one. Formally, it can be written as

$$\omega \mathcal{A}\delta(x) = \mathcal{B}\delta(x), \tag{15}$$

where $\mathcal{A}$ and $\mathcal{B}$ are integro-differential operators.

The numerical implementation of the stability calculation consists of first interpolating the steady-state solution to a vector of size N_{pts} (typically, $N_{pts} \sim 300$). For better results, it was necessary to get a higher density of discretization points at the tails. To maintain accuracy, the partition of discretization points, x_i, was calculated using the parameterization

$$x(w) = x_0 + \Delta \frac{\tanh \rho w}{\tanh \rho}, \tag{16}$$

where w_i is the computational axis varying from -1 to 1, and ρ is an adjustable parameter.

Next, the $N_{pts} \times N_{pts}$ stability operators, $\mathcal{A}$ and $\mathcal{B}$, were calculated. The derivatives were replaced by the standard three-point discretization, whereas the integrals were again evaluated by the trapezoidal rule after accounting for the singular pieces. Finally, we solved the linear eigenvalue problem using the EISPACK Library routine DRGG. This routine solves the equation directly without going through the inversion of $\mathcal{A}$, which proved to induce large numerical errors [21,22].

4. Steady state solutions

4.1. Symmetric dendrites

The essence of our results is presented in Figs. 3a-3c, where the Péclet number of each of the multiple steady-state solutions is plotted versus supersaturation. With respect to symmetric fingers, for which an approximate theory exists, our results provide a new picture. The approximate analytical treatment of Brener *et al.* [2] predicts that branches are formed by connecting the nth dendritic-like (high p) solutions to the nth Saffman-Taylor-like (low p) solutions. By dendritic-like, it is meant that p is an increasing function of Δ, unlike the Saffman-Taylor like solutions. Thus, the nth branch was predicted to be wholly contained in the $n-1$ branch. Brener *et al.* also gave a convincing argument for why only the dendritic-like solution could be stable.

The first of these predictions is not borne out for low anisotropy, as well as for large surface tension (which, from dimensional considerations, is equivalent to a narrow channel). For $\epsilon = 0.1$ (Fig. 3c), the $n = 0$ branch is in accord with the prediction,

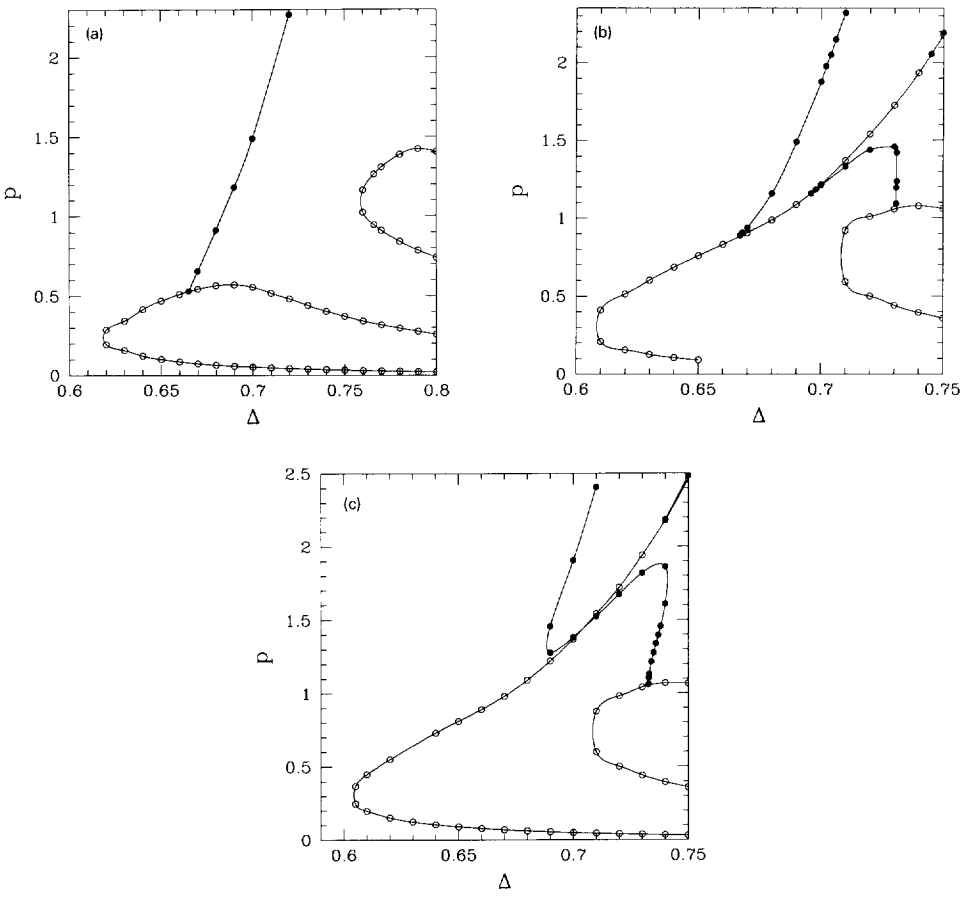

Fig. 3. Péclet number versus supersaturation for steady state solutions of parity-broken dendrites (filled dots) and symmetric dendrites (open dots). The parameters are $d_0 = 0.01$ and (a) $\epsilon = 0$, (b) $\epsilon = 0.09$ and (c) $\epsilon = 0.1$.

however all the higher branches which are inside the main branch are Saffman-Taylor-like. Thus, the next branch connects the $n = 1$ and $n = 2$ Saffman-Taylor solutions, followed by a branch connecting the $n = 3$ and $n = 4$ Saffman-Taylor solutions, etc. For $\epsilon = 0$ (Fig. 3a), all the branches of the symmetric solutions are Saffman Taylor like, but this time it is the $n = 0$ and $n = 1$ solutions which are connected, then, the $n = 2$ and $n = 3$ solutions, etc. Clearly, a continuous transition between these two pictures as anisotropy is decreased, must go through the merging and the reconnection of branches. In Fig. 4 we show the $p(\Delta)$ curves for the symmetric solutions for $\epsilon = 0.08$. Compared to the $\epsilon = 0.1$ picture, the Saffman-Taylor solutions remain practically unchanged, while the main dendritic branch merges with the $n = 1$ branch and the two reconnect. Hence, for $\epsilon = 0.08$, the $n = 0$ and $n = 1$ Saffman-Taylor solutions are connected, while the main dendritic solution is connected to the $n = 2$ Saffman-Taylor solution. This process of merging and reconnection of the main dendritic solution with the higher Saffman-Taylor

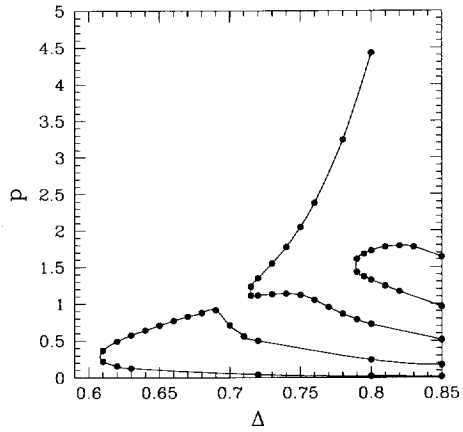

Fig. 4. Péclet number versus supersaturation for symmetric dendrites for $d_0 = 0.01$ and $\epsilon = 0.08$.

branches goes on as anisotropy is further decreased. Presumably, an inverse process occurs for increasing anisotropy or for decreasing surface tension, giving rise to the formation of higher dendritic branches. Clearly, for any finite amount of anisotropy, the entire discrete set of free dendrites must be recovered in the limit of infinite channel width.

Brener *et al.*'s approach, while very useful, does not enable to capture the intricacies of this merging and reconnection. This is presumably due to the nature of their approximation for the zero-surface-tension solution which does not capture the true singularity structure in the complex plane. A similar merging and reconnection were found in the case of the Saffman-Taylor sector problem to result from the existence of branch-cut singularities of the zero-surface-tension solution [23]. Verifying such a singularity structure in the present problem is an interesting challenge for the future.

4.2. *Parity-broken dendrites*

In addition to the symmetric solutions, we also obtained steady-state parity-broken dendrites (Fig. 6). As a first verification, we compared our solutions to the dynamical results of Ref. [10]. The agreement is fairly good, keeping in mind that the latter is for a non-conserved order-parameter.

For isotropic surface tension (Fig. 3a), one branch of parity-broken solutions was obtained. It originates from the main branch of the symmetric solutions at $\Delta \approx 0.665$ through a forward bifurcation (the asymmetry vanishes as the two solutions merge) (Fig. 5). The Péclet number, p, increases rapidly with Δ, hence, the parity-broken solutions are presumably the ones which are dynamically selected.

For $\epsilon = 0.09$, two additional branches of parity-broken solutions were found. Both also bifurcate from branches of symmetric solutions. The first originates from the main dendritic branch at $\Delta \approx 0.745$, through a forward bifurcation, whereas the second connects the main dendritic branch to the $n = 1$ symmetric branch. For slightly higher anisotropy,

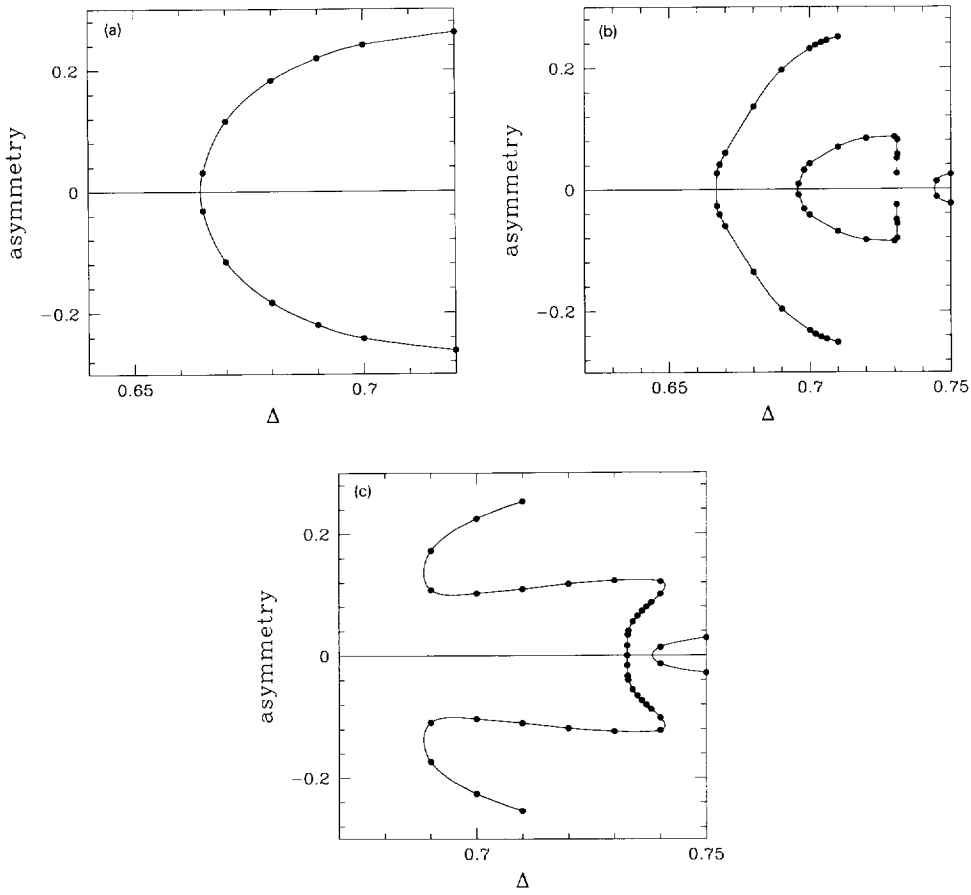

Fig. 5. A measure of the asymmetry of the parity-broken dendrites, $(\lambda_2-\lambda_1)/(\lambda_2+\lambda_1)$, versus supersaturation for $d_0 = 0.01$ and (a) $\epsilon = 0$, (b) $\epsilon = 0.09$ and (c) $\epsilon = 0.1$.

the bifurcation point of this second branch merges with the original bifurcation point to form a new branch which is disconnected from the symmetric solutions. This new branch structure is obtained for $\epsilon = 0.1$ (Figs. 3c,5c).

The above results settle the puzzle of the origin of the parity-broken dendrites. If all the steady-state solutions are represented on hypersurfaces in the three-dimensional space of control parameters, (Δ, d_0, ϵ), then the parity-broken solutions are analytically connected to the symmetric ones, arising from standard bifurcations. Only along cuts in the parameters space, such as the $p(\Delta)$ curves, the symmetric and the asymmetric solutions can be disconnected.

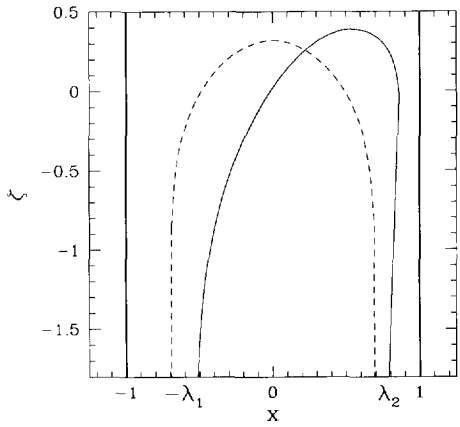

Fig. 6. Steady-state solutions of a parity-broken dendrite (solid) and a symmetric dendrite (dashed) in a channel for $d_0 = 0.01$, $\epsilon = 0$ and $\Delta = 0.7$. The velocity and the transversal location of the parity-broken dendrite are $p = 1.48$ and $\lambda_2 = 0.869$. The velocity of the symmetric dendrite is $p = 0.56$.

5. Linear stability

For all the steady-state solutions, we performed the linear stability calculations. The spectrum consists of three distinct pieces, as was already found for free dendrites [21] and for Saffman-Taylor fingers [22]. At large negative $\mathrm{Re}\,\omega$, there is a real continuum, ending at a point on the negative $\mathrm{Re}\,\omega$ axis. From there emerges a complex continuum, followed by real discrete modes. A discrete zero mode is always present due to the translational invariance. As we parameterize our perturbations by δz, the longitudinal shift, the translation zero-mode is completely decoupled (contrasting with using δn), and so cannot be used as a measure of the accuracy of the procedure. The unstable modes all belong to the discrete spectrum, therefore we consider below only the discrete eigenmodes in the vicinity of the stability threshold. If represented as normal shifts, these modes are decaying towards the boundaries, hence correspond to tip instabilities.

The main goal is to understand the spectral flow associated with the main branches of solutions, and in particular between the symmetric and the parity-broken solutions. In Table 1 we present the leading eigenmodes on the $n = 0$ symmetric and parity-broken branches for $\epsilon = 0$. Below the bifurcation point, $\Delta \lesssim 0.665$, the branch of symmetric solutions is linearly stable. At the bifurcation point, it picks up one unstable anti-symmetric mode. Thus, the stability is transferred to the branch of the parity-broken solutions. At $\Delta \approx 0.69$, it acquires a second unstable mode, this time a symmetric one. This instability occurs at the point where p becomes a decreasing function of Δ, in accord with the argument of Brener *et al.* [2]. The branch of parity-broken solutions is stable as befits a forward bifurcation. To summarize, these is a stable symmetric solution for $0.62 \lesssim \Delta \lesssim 0.665$, and a stable parity-broken solution for larger Δ.

In Table 2 we present the leading eigenmodes on the main symmetric branch for $\epsilon = 0.09$. At the main bifurcation point, $\Delta \approx 0.665$, the same scenario repeats, namely, the

Table 1
Data for the leading eigenmodes on the symmetric and the parity-broken main branches for $\epsilon = 0$. ω_S and ω_A denotes symmetric and anti-symmetric modes respectively

	Δ	p	ω_A	ω_S
Symmetric dendrites	0.65	0.47	−0.11	−0.65
	0.66	0.51	−0.06	−0.61
	0.67	0.55	+0.03	−0.47
	0.68	0.57	+0.15	−0.25
	0.69	0.57	+0.33	+0.02
	0.70	0.56	+0.54	+0.28
			ω	
Parity-broken dendrites	0.67	0.66	−0.47	
	0.68	0.91	−0.90	
	0.69	1.18	−1.57	
	0.70	1.48	−2.52	

Table 2
Data for the leading eigenmodes on the main symmetric branch for $\epsilon = 0.09$

Δ	p	ω_A	ω_S
0.64	0.69	−0.12	−1.30
0.65	0.76	−0.08	−1.25
0.66	0.83	−0.03	−1.17
0.67	0.91	+0.01	−1.10
0.68	0.99	+0.05	−1.10
0.69	1.09	+0.03	−1.35
0.70	1.21	−0.04	−2.12
0.71	1.37	−0.09	−2.82
0.72	1.54	−0.10	−3.12

symmetric solutions are stable below it, and pick up an unstable mode at the bifurcation point. The stability is transferred to the parity-broken solutions. Here, the stability of the symmetric solutions is recovered at the second bifurcation point, $\Delta \approx 0.696$. The unstable mode is transferred to the emerging parity-broken branch. Thus, except for a short interval between the two bifurcation points, both the symmetric and the parity-broken solution are linearly stable till the next bifurcation off the symmetric branch is encountered at $\Delta \approx 0.745$. This interval of instability shrinks as the bifurcation points merge, and disappear when the parity-broken solutions disconnect from the symmetric ones.

6. Discussion

In this paper, we have shown that the new class of parity-broken fingers growing during solidification in a channel are analytically connected to the symmetric solutions.

The branches of parity-broken solutions emerge through standard bifurcations. For sufficiently strong anisotropy, two of such branches can merge, and disconnect from the symmetric branch. Such parity-broken solutions exist for $\Delta > \Delta_c(d_0, \epsilon)$.

We have found that the fastest parity-broken branch is stable for all parameters we have investigated. The symmetric branch is stable for Δ up to the first bifurcation. This region grows as the anisotropy is increased. Thus, we confirm the coexistence of two stable patterns on a wide range of parameters.

Ihle and Müller-Krumbhaar report that at sufficiently large anisotropy, the symmetric branch appears to intersect the parity-broken one, beyond which point a stable parity-broken solution was not found. For $d_0 = 0.01$, we found no such crossing up to $\epsilon = 0.28$. One needs to investigate this point further, in particular for smaller d_0 corresponding to the values used by Ihle and Müller-Krumbhaar. We did see however that as ϵ increased, the eigenvalue of the least stable mode increased reaching a local maximum before turning back down again. Thus, it is conceivable that at lower values of d_0 the eigenvalue might occasionly cross zero.

Another open question is the possibility for fingers to grow even in directions other than the directions of minimum surface tension. Ihle and Müller-Krumbhaar obtained fingers for which the growth direction was at an angle of 8.7° with respect to the natural growth direction. On theoretical grounds, this is not surprising as parity-broken solutions exist even in the absence of anisotropy. A similar phenomenon happens in Saffman-Taylor fingers [24]. The stability of such "misoriented" fingers is worthy of further study.

The most difficult set of questions that need to be addressed are those concerning pattern selection and morphology transitions. In a given channel, many different patterns are possible in principle. For example, for sufficiently large anisotropy the system has to select between symmetric and parity-broken fingers. One consideration is the relative size of the basins of attraction of the two solutions. The other is the non-linear stability/insensitivity to noise of the two patterns. In addition, there is the possibility of multiple fingers in a given channel [9]. Of course, knowing the result for $p(d_0, \Delta, \epsilon)$ allows us to directly find the velocity of the n-fingers solution,

$$v_{(n)} = \frac{2D}{a} n\, p(n\, d_0/a, \Delta, \epsilon). \tag{17}$$

For the symmetric fingers, we know that this function has a maximum [2]. Presumably, the same holds true for the parity-broken case as well. It would be interesting to see if the selected channel width is such that the system operates at the maximum velocity [13].

Acknowledgement

We are grateful to H. Levine, I. Aranson, O. Shochet, M. Azbel and R. Mints for useful discussions. We thank H. Müller-Krumbhaar for a critical reading of the manuscript and

his valuable comments. We acknowledge the support of the US-Israel Binational Science Foundation. This study was partially supported by a grant from the G.I.F., the German-Israeli Foundation for Scientific Research and Development. DAK is a Guastella Fellow, supported by the Raschi Foundation.

References

[1] D.A. Kessler, J. Koplik and H. Levine, Phys. Rev. A 34 (1986) 4980.
[2] E. Brener, M. Geilikman and D. Temkin, Sov. Phys. JETP 67 (1988) 1002.
[3] D.A. Kessler, J. Koplik and H. Levine, Adv. Phys. 37 (1988) 255.
[4] J.S. Langer, Science 243 (1989) 1150.
[5] E. Ben-Jacob and P. Garik, Nature 343 (1990) 523.
[6] E.A. Brener and V.I. Mel'nikov, Adv. Phys. 40 (1991) 53.
[7] M. Ben-Amar and Y. Pomeau, Europhys. Lett. 2 (1986) 307.
[8] D.A. Kessler, J. Koplik and H. Levine, Phys. Rev. A 33 (1986) 3352.
[9] E. Brener, H. Müller-Krumbhaar, Y. Saito and D.E. Temkin, Phys. Rev. E 47 (1993) 1151.
[10] T. Ihle and H. Müller-Krumbhaar, Phys. Rev. Lett. 70 (1993) 3083; Phys. Rev. E 49 (1994) 2972.
[11] R. Kupferman, O. Shochet and E. Ben-Jacob, Phys. Rev. E 50 (1994) 1005.
[12] E. Ben-Jacob, G. Deutscher, P. Garik, N. Goldenfeld and Y. Lareah, Phys. Rev. Lett. 57 (1986) 1903.
[13] E.A. Brener, H. Müller-Krumbhaar and D.E. Temkin, Europhys. Lett. 17 (1992) 535.
[14] E. Ben-Jacob, P. Garik, T. Muller and D. Grier, Phys. Rev. A 38 (1988) 1370.
[15] O. Shochet and E. Ben-Jacob, Phys. Rev. E 48 (1993) 4168.
[16] O. Shochet, K. Kassner, E. Ben-Jacob, S.G. Lipson and H. Müller-Krumbhaar, Physica A 181 (1992) 136; 187 (1992) 87.
[17] S. Tanveer, Phys. Fluids 30 (1987) 1589.
[18] K. Kassner, A. Valance, C. Misbah and D.E. Temkin, Phys. Rev. E 48 (1993) 1091.
[19] W-J. Rappel, Phys. Rev. E 48 (1993) 4118.
[20] P. Coullet, R. Goldstein and G.H. Gunaratne, Phys. Rev. Lett. 63 (1989) 1954.
[21] D.A. Kessler and H. Levine, Phys. Rev. Lett. 57 (1986) 3069.
[22] D.A. Kessler and H. Levine, Phys. Fluids 30 (1987) 1246.
[23] M. Ben-Amar, Phys. Rev. A 44 (1991) 3673.
[24] R. Combescot, Phys. Rev. E 49 (1994) 4172.